C2C12 cell sheets by adding DMEM into the upper section of the device and glucose/pyruvic acid–deficient DMEM into the lower part. The permeabilities of pyruvic acid and glucose were inhibited by approximately 60% (in other words, it was reduced to approximately 40%) by a single-layered C2C12 cell sheet (Fig. 3A, B). As the number of layered cell sheets increased, the permeabilities of pyruvic acid and glucose decreased. Almost complete inhibition of the permeability was observed upon the use of a quadruple-layered or a quintuple-layered cell sheet (Fig. 3A, B). Similar results were also observed using EMC sheets (Fig. 3D, E).

In the next set of experiments, the permeabilities of creatinin, β2-microgloblin, and transferrin were examined, because these are important substances for measuring the kidney glomerulus function.[25,26] DMEM containing creatinin, β2-microglobulin, or transferrin was added to the upper part of the device, while DMEM without these substances was added to the lower part. The permeability of creatinin was inhibited by approximately 50% by a single-layered C2C12 cell sheet (Fig. 3C). Again, as the number of layered cell sheets increased, the sheets' collective inhibitory effects increased. The permeability of creatinin was inhibited by approximately 85% by a quintuple-layered cell sheet (Fig. 3C). On the other hand, the permeabilities of β2-microglobulin and transferrin were inhibited by approximately 80% and 90% by only a single-layered C2C12 cell sheet, respectively, and both were almost completely inhibited by a double-layered cell sheet (Fig. 4A, B). Similar results were also observed using EMC sheets (Figs. 3F and 4D, E).

In the third set of experiments, the permeabilities of VEGF and SDF-1α were examined, because these substances are important in the regeneration of tissues.[27,28] DMEM containing either SDF-1α or VEGF was added to the upper part of the device, while DMEM was added to the lower part. C2C12 cells secreted SDF-1α, and EMCs secreted VEGF, but not SDF-1α (data not shown). A human-specific VEGF ELISA kit, which is unable to cross react with mouse VEGF, was used to detect VEGF. Therefore, only C2C12 cell sheets were used for determining the permeability of VEGF, and only EMC sheets were used for determining the permeability of SDF-1α. The permeability of VEGF was inhibited by approximately 95% (in other words, it was reduced to 5%) by a single-layered C2C12 cell sheet and was almost completely inhibited by a double-layered cell sheet (Fig. 4C). Likewise, the permeability of SDF-1α was inhibited by approximately 90% by a single-layered EMC sheet and was almost completely inhibited by a double-layered cell sheet (Fig. 4F).

The rate of consumption of glucose and pyruvic acid increased as the number of cell sheets increased. Once tissues had more than triple-layered cell sheets, the increase of the rate slowed (Fig. 5A, B). Similar tendency was also observed in the experiments using EMC sheets (Fig. 5C, D). In contrast, the amount of creatinin, SDF-1α, VEGF, β2-microglobulin, and transferrin was hardly changed during incubation with layered cell sheets (data not shown).

Discussion

Many reports have already been published regarding the permeability and uptake of various substances through a single-layered of cells.[1–5] The present study is unique and original because our new assay system can measure the permeability of substances through cell-dense 3D tissues rather than a single-layered of cells. The cell-dense 3D tissue was prepared by cell sheet engineering, and the device was made by our laboratory.

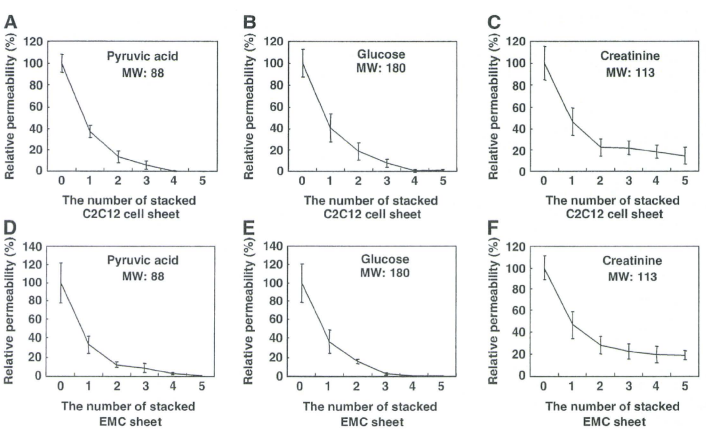

FIG. 3. Permeability of low-molecular-weight substances. The graph (**A**) shows pyruvic acid experiment through C2C12 cell sheets; (**B**), glucose; and (**C**), creatinin. The graph (**D**) shows pyruvic acid experiment through EMC sheets; (**E**), glucose; and (**F**), creatinin. The data are expressed as mean ± SD ($n = 4$).

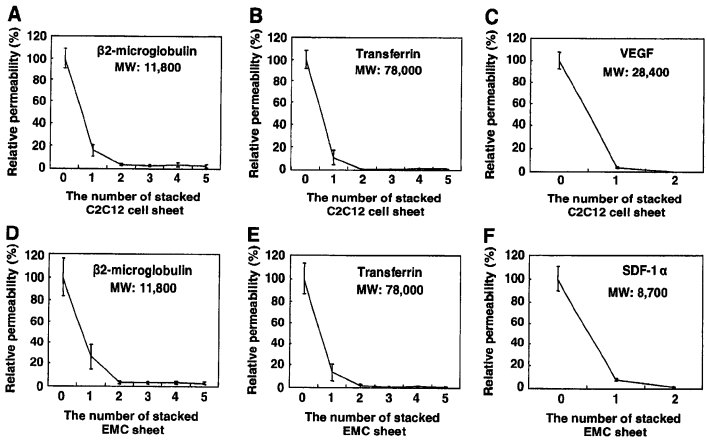

FIG. 4. Permeability of high-molecular-weight substances. The graph (A) shows β2-microglobulin experiment through C2C12 cell sheets; (B), transferrin; and (C), VEGF. The graph (D) shows β2-microglobulin experiment through EMC sheets; (E), transferrin; and (F), SDF-1α. The data are expressed as mean ± SD ($n = 4$).

First, we used our assay system to examine the permeability of nutrients across 3D tissues (Fig. 3). The results suggested that the cells that were separated from their nutrient source by more than triple-layered cell sheets were severely starved of nutrients. Both *in vivo* and *in vitro*, cell death was found to be common in engineered tissues of more than triple-layered cell sheets, though the same kinds of cells usually survive without necrosis in tissues consisting of a single-, a double-, or a triple-layered cell sheet[29] (Sekine, W., Haraguchi, Y., Shimizu, T., Umezawa, A., and Okano, T.,

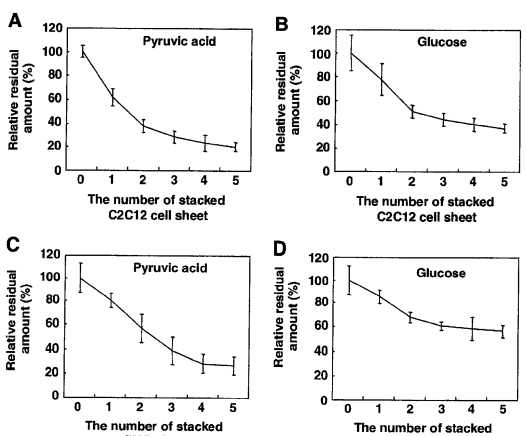

FIG. 5. Consumption of nutrients during incubation with layered cell sheets. The graph (A) shows relative residual amount of pyruvic acid after incubation with C2C12 cell sheets, and (B) shows that of glucose. The graph (C) shows relative residual amount of pyruvic acid after incubation with EMC sheets, and (D) shows that of glucose. The amounts of substances taken after 24 h without the cell sheet were assumed to be 100%. The data are expressed as mean ± SD ($n = 4$).

unpublished observation). Our results suggested that insufficient diffusion of nutrients induces a rapid cell death in the thick tissues. Other reports, in contrast, have claimed that glucose could penetrate into 3D tissues via a scaffold containing skeletal muscle myoblasts.[30] The report showed that glucose concentrations only decreased from 4.28 mmol/L at the edge of the tissue to 3.18 mmol/L at the depth of 2 mm.[30] This result is profoundly different from ours; the inconsistency is probably due to different cell densities of 3D tissues of the two studies. In this study, 3D tissues, which were fabricated by cell sheet engineering, were constructed without 3D scaffolds described above and were, therefore, very cell dense. In contrast, in the reported study, 3D tissues fabricated using scaffolds were very cell sparse due to insufficient cell migration into the scaffolds. Nevertheless, both our study and that of Davis *et al.*[30] present important data that are relevant to the field of tissue metabology.

In another set of experiments, the permeability of high-molecular-weight substrates (SDF-1α, VEGF, β2-microglobulin, and transferrin) was completely inhibited by a double-layered cell sheet. These results show that cells in tissues that are only one or two layers thick can be deficient in growth factors or cytokines. We propose that the formation of functional microvessels is necessary to supply these large molecules into the interiors of 3D tissues. On the other hand, VEGF and SDF-1α have received a great deal of attention from the field of regenerative medicine.[27,28] The former is intimately involved in angiogenesis, and the latter with stem cell homing. In fact, VEGF has even been used in clinical therapy, and in animal experiment; SDF-1α could improve myocardial function after infarction.[26,28] It is thought that the effectiveness of these factors depends on the efficiency of diffusion into the treated area. In the present study, we showed that these factors were unable to diffuse efficiently into the cell-dense tissues. Thus, the successful implementation of cytokine therapy will require a development of techniques that can help these factors diffuse efficiently. Our assay system using cell-dense 3D tissues may be useful for the development of efficient cytokine therapy.

In this article, the permeability of substances through cell-dense 3D tissue was shown to be significantly reduced depending on the molecular weight (Figs. 3 and 4). This observation agrees with a report that the permeability of mannitol (molecular weight: 182) through a single-layered of brain capillary endothelial cell lines on a cell culture insert was approximately twice as great as that of inulin (molecular weight: 5,000).[2] These results showed that the permeability of substances through 2D cell culture and 3D tissues was significantly reduced with the increase of molecular weight, and that our assay system is feasible as an assay system to measure the permeability of substances through 3D tissues.

Drug development requires the development of *in vitro* assay systems that simulate actual living tissues and organs. In addition, an adequate assay system has a clear advantage as an *in vitro* model that require no animal experiments. The researcher should try as much as possible to replace the animal model with an alternative nonanimal model.[31] It is generally thought that 3D culture systems resemble *in vivo* situations much more closely than 2D culture systems.[7,10,11] Cell sheet engineering gives the fabrication of cell-dense 3D tissues without biodegradable scaffolds. Therefore, for example, layered cardiomyocyte sheets interact directly with each other and can couple electrically, resulting in synchronously beating 3D myocardial tissues *in vitro*.[32,33] *In vivo* subcutaneous transplantation of layer cardiomyocyte sheets also demonstrated that these synchronously beating heart-like tissues survive for over 1 year.[33] Our *in vitro* 3D assay system using cell sheet engineering is thought to be proper for *in vivo* situation. Therefore, our assay system has potential to reduce animal experiment. In addition, the cell sheet engineering also enables the fabrication of complicated heterogeneous tissues. In fact, our laboratory previously reported about heterogeneous 3D coculture comprising hepatocytes and endothelial cells using the technique.[34] The hepatocytes of the 3D culture system showed a differentiated cell shape and the extensive albumin expression of hepatocytes, which were never seen in hepatocyte monoculture.[34] Combination of our assay system and heterogeneous layering cell sheets can allow us to analyze pharmacologically and pharmacokinetically complicated 3D tissues such as the blood–brain barrier, the small intestinal mucosa, and the kidney glomerulus. For example, the blood–brain barrier model can be fabricated by a combination of an endothelial cell sheet, a pericyte sheet, and an astrocyte sheet.

Several novel therapies containing a hybrid bioartificial kidney for the treatment of kidney failure are tried clinically.[35] The hybrid bioartificial kidney is combined with dialysis membrane and cells. In this study a device by modifying a cell culture insert was used. By the replacement of the device dialysis membrane and cell sheet, a new hybrid-type artificial kidney model device can also be fabricated easily. Therefore, our assay system may be applied in the field of dialysis membrane technology.

Conclusions

We have developed a new model system that measures the permeability of substances through cell-dense 3D tissues using cell sheet engineering and a modified cell culture insert, and analyzed in detail the permeability of various molecules. It has been shown that our assay system is feasible as an assay system to measure the permeability of substances through 3D tissues using substances that have various molecular weights. This is the first report about measuring the permeability of substances through cell-dense 3D tissues without scaffolds. The thickness of the tissues can be also controlled easily as shown in Figure 2. Our assay system represents a significant advancement and offers much exciting potential in the fields of biochemistry, physiology, metabology of tissues, cytokine therapy, drug development, and dialysis membrane technology.

Acknowledgments

We appreciate the useful comments and technical criticism of Drs. Norio Ueno and Noriaki Matsuda (Institute of Advanced Biomedical Engineering and Science, Tokyo Women's Medical University). This work was supported by grants from the 21COE program and the High-Tech Research Center Program from the Ministry of Education, Culture, Sports, Science, and Technology; grants from the Japan Society for the Promotion of Science; Research Grants for Cardiovascular Disease and Regenerative Medicine from the

Ministry of Health, Labour, and Welfare; and the Open Research Grant from the Japanese Research Promotion Society for Cardiovascular Diseases.

Disclosure Statement

No competing financial interests exist.

References

1. Hilgers, A.R., Conradi, R.A., and Burton, P.S. Caco-2 cell monolayers as a model for drug transport across the intestinal mucosa. Pharm Res **7,** 902, 1990.
2. Hosoya, K., Tetsuka, K., Nagase, K., Tomi, M., Saeki, S., Ohtsuki, S., Takanaga, H., Yanai, N., Obinata, M., Kikuchi, A., Okano, T., and Terasaki, T. Conditionally immortalized brain capillary endothelial cell lines established from a transgenic mouse harboring temperature-sensitive simian virus 40 large T-antigen gene. AAPS Pharm Sci **2,** E27, 2000.
3. Kimura, T., Yamano, H., Tanaka, A., Matsumura, T., Ueda, M., Ogawara, K., and Higaki, K. Transport of D-glucose across cultured stratified cell layer of human oral mucosal cells. J Pharm Pharmacol **54,** 213, 2002.
4. Roux, F., and Couraud, P.O. Rat brain endothelial cell lines for the study of blood-brain barrier permeability and transport functions. Cell Mol Neurobiol **25,** 41, 2005.
5. Tomi, M., Terayama, T., Isobe, T., Egami, F., Morito, A., Kurachi, M., Ohtsuki, S., Kang, Y.S., Terasaki, T., and Hosoya, K. Function and regulation of taurine transport at the inner blood-retinal barrier. Microvasc Res **73,** 100, 2007.
6. Mukhopadhyay, P., Rajesh, M., Bátkai, S., Kashiwaya, Y., Haskó, G., Liaudet, L., Szabó, C., and Pacher, P. Role of superoxide, nitric oxide, and peroxynitrite in doxorubicin-induced cell death *in vivo* and *in vitro*. Am J Physiol Heart Circ Physiol **296,** 1466, 2009.
7. Abbott, A. Biology's new dimension. Nature **424,** 870, 2003.
8. Brännvall, K., Bergman, K., Wallenquist, U., Svahn, S., Bowden, T., Hilborn, J., and Forsberg-Nilsson, K. Enhanced neuronal differentiation in a three-dimensional collagen-hyaluronan matrix. J Neurosci Res **85,** 2138, 2007.
9. Liu, H., Collins, S.F., and Suggs, L.J. Three-dimensional culture for expansion and differentiation of mouse embryonic stem cells. Biomaterials **27,** 6004, 2006.
10. Editorial. Goodbye, flat biology? Nature **424,** 861, 2003.
11. Smalley, K.S., Lioni, M., and Herlyn, M. Life isn't flat: taking cancer biology to the next dimension. In Vitro Cell Dev Biol Anim **42,** 242, 2006.
12. Langer, R., and Vacanti, J.P. Tissue engineering. Science **260,** 920, 1993.
13. Leor, J., Aboulafia-Etzion, S., Dar, A., Shapiro, L., Barbash, I.M., Battler, A., Granot, Y., and Cohen, S. Bioengineered cardiac grafts: a new approach to repair the infracted myocardium? Circulation **100(suppl II),** II63, 1999.
14. Sakai, T., Li, R.K., Weisel, R.D., Mickle, D.A., Kim, E.T., Jia, Z.Q., and Yau, T.M. The fate of a tissue-engineered cardiac graft in the right ventricular outflow tract of the rat. J Thorac Cardiovasc Surg **121,** 932, 2001.
15. Yamato, M., and Okano, T. Cell sheet engineering. Materials Today **7,** 42, 2004.
16. Yamada, N., Okano, T., Sakai, H., Karikusa, F., Sawasaki, Y., and Sakurai, Y. Thermo-responsive polymeric surface: control of attachment and detachment of cultured cells. Makromol Chem Rapid Commun **11,** 571, 1990.
17. Okano, T., Yamada, N., Sakai, H., and Sakurai, Y. A novel recovery system for cultured cells using plasma-treated polystyrene dishes grafted with poly (N-isopropylacrylamide). J Biomed Mater Res **27,** 1243, 1993.
18. Yang, J., Yamato, M., Shimizu, T., Sekine, H., Ohashi, K., Kanzaki, M., Ohki, T., Nishida, K., and Okano, T. Reconstruction of functional tissues with cell sheet engineering. Biomaterials **28,** 5033, 2007.
19. Matsuda, N., Shimizu, T., Yamato, M., and Okano, T. Tissue engineering based on cell sheet technology. Adv Mater **19,** 3089, 2007.
20. Yamato, M., Utsumi, M., Kushida, A., Konno, C., Kikuchi, A., and Okano, T. Thermo-responsive culture dishes allow the intact harvest of multilayered keratinocyte sheets without dispase by reducing temperature. Tissue Eng **7,** 473, 2001.
21. Nishida, K., Yamato, M., Hayashida, Y., Watanabe, K., Maeda, N., Watanabe, H., Yamamoto, K., Nagai, S., Kikuchi, A., Tano, Y., and Okano, T. Functional bioengineered corneal epithelial sheet grafts from corneal stem cells expanded *ex vivo* on a temperature-responsive cell culture surface. Transplantation **77,** 379, 2004.
22. Hida, N., Nishiyama, N., Miyoshi, S., Kira, S., Segawa, K., Uyama, T., Mori, T., Miyado, K., Ikegami, Y., Cui, C., Kiyono, T., Kyo, S., Shimizu, T., Okano, T., Sakamoto, M., Ogawa, S., and Umezawa, A. Novel cardiac precursor-like cells from human menstrual blood-derived mesenchymal cells. Stem Cells **26,** 1695, 2008.
23. Koch, C.D. Determination of glucose with glucoseoxidase-UV, using hexokinase as the reference method. J Clin Chem Clin Biochem **14,** 373, 1976.
24. Valero, E., and García-Carmona, F. Optimizing enzymatic cycling assays: spectrophotometric determination of low levels of pyruvate and L-lactate. Anal Biochem **239,** 47, 1996.
25. Boron, W.F., and Boulpaep, E.L. Medical Physiology. Philadelphia, PA: Elsevier Science, 2003.
26. Branten, A.J., Swinkels, D.W., Klasen, I.S., and Wetzels, J.F. Serum ferritin levels are increased in patients with glomerular diseases and proteinuria. Nephrol Dial Transplant **19,** 2754, 2004.
27. Tang, J., Wang, J., Song, H., Huang, Y., Yang, J., Kong, X., Guo, L., Zheng, F., and Zhang, L. Adenovirus-mediated stromal cell-derived factor-1 alpha gene transfer improves cardiac structure and function after experimental myocardial infarction through angiogenic and antifibrotic actions. Mol Biol Rep (in press).
28. Gaffney, M.M., Hynes, S.O., Barry, F., and O'Brien, T. Cardiovascular gene therapy: current status and therapeutic potential. Br J Pharmacol **152,** 175, 2007.
29. Shimizu, T., Sekine, H., Yang, J., Isoi, Y., Yamato, M., Kikuchi, A., Kobayashi, E., and Okano, T. Polysurgery of cell sheet grafts overcomes diffusion limits to produce thick, vascularized myocardial tissues. FASEB J **20,** 708, 2006.
30. Davis, B.H., Schroeder, T., Yarmolenko, P.S., Guilak, F., Dewhirst, M.W., and Taylor, D.A. An *in vitro* system to evaluate the effects of ischemia on survival of cells used for cell therapy. Ann Biomed Eng **35,** 1414, 2007.
31. Vitale, A., Manciocco, A., and Alleva, E. The 3R principle and the use of non-human primates in the study of neurodegenerative diseases: the case of Parkinson's disease. Neurosci Biobehav Rev **33,** 33, 2009.
32. Shimizu, T., Yamato, M., Isoi, Y., Akutsu, T., Setomaru, T., Abe, K., Kikuchi, A., Umezu, M., and Okano T. Fabrication of

pulsatile cardiac tissue grafts using a novel 3-dimensional cell sheet manipulation technique and temperature-responsive cell culture surfaces. Circ Res **90,** e40, 2002.
33. Shimizu, T., Yamato, M., Kikuchi, A., and Okano, T. Cell sheet engineering for myocardial tissue reconstruction. Biomaterials **24,** 2309, 2003.
34. Harimoto, M., Yamato, M., Hirose, M., Takahashi, C., Isoi, Y., Kikuchi, A., and Okano, T. Novel approach for achieving double-layered cell sheets co-culture: overlaying endothelial cell sheets onto monolayer hepatocytes utilizing temperature-responsive culture dishes. J Biomed Mater Res **62,** 464, 2002.
35. Fissell, W.H. Developments towards an artificial kidney. Expert Rev Med Devices **3,** 155, 2006.

Address correspondence to:
Teruo Okano, Ph.D.
Institute of Advanced Biomedical Engineering and Science
TWIns, Tokyo Women's Medical University
8-1 Kawada-cho, Shinjuku-ku
Tokyo 162-8666
Japan

E-mail: tokano@abmes.twmu.ac.jp

Received: July 6, 2009
Accepted: September 28, 2009
Online Publication Date: November 9, 2009

A Study of Micro-bubble Enhanced Ultrasound Gene Induction

A. Okamoto[1], R. Tachibana[1], K. Yoshinaka[2], K. Osada[3], S. Takagi[1], K. Kataoka[2,3], U. Chung[2], and Y. Matsumoto[1]

[1] Department of Mechanical Engineering, The University of Tokyo, Tokyo, Japan
[2] Department of Bioengineering, The University of Tokyo, Tokyo, Japan
[3] Department of Materials Engineering, The University of Tokyo, Tokyo, Japan

Abstract— **Recently, a development of the ultrasound gene induction system, called Sonoporation has been investigated. It is known that micro-bubbles can help gene transfection. It is thought that genes are inducted into cells by collapses of cavitation-bubble or micro-bubble. However, the mechanism and optimal induction condition have not been clarified in detail. In this research, we improve gene induction rate by forming DNA/Block copolymer micelle. By forming micelle, DNA is compacted and the stability of DNA is improved. Therefore, it is expected that DNA become able to pass through a hole on cells easily and the expression ability of genes is advanced. Ultrasonic plane wave is exposured from PZT transducer. The frequency is 2MHz and Duty Cycle is 10% (40/360). Mouse fibroblast cell line (NIH3T3) is cultured on the bottom of 24-well plate. We add plasmid DNA and Micro-bubble to culture solution and then exposure ultrasound from above the cells. We use GFP plasmid as reporter gene, and Sonazoid® as micro-bubble. Micelle is formed by combining DNA and block copolymer. Block copolymer is composed of polyethyleneglycol-group and poly-lysine. Each naked DNA and polymer micelle is added to culture medium with microbubble, and then exposure ultrasound. Experimental conditions are set as follows: plasmid density is 15μg/ml, number density of microbubble is 1.7×10^5 count/mm^3, ultrasound intensity is 10.2 W/cm^2, ultrasound exposure time is 60 seconds, and sample number is 12. As a result, Gene induction ratio is doubled by forming polymer micelle (from about 1% to about 1.7%). Therefore, the availability of forming polymer micelle is confirmed.**

Keywords— **Ultrasonic therapy, Gene therapy, Gene induction, Buble, Cavitation.**

I. Introduction

Gene therapy is an approach for treating diseases caused by a gene abnormality or deficit. However, gene therapy requires the induction of genes into cells. Various systems to accomplish this have already been devised—for example, viral vectors [1], electroporation [2] and lipofection [3]—but these methods are associated with several problems. Viral vectors have reportedly caused leukemia. Electroporation is not practical for tissues within the body, as the method would require dissection of the affected area and direct application of voltage, while performing gene induction in vitro would require the cells to be delivered to the affected area. Thus, this approach is invasive and would cause patient distress. Lipofection is associated with an unstability of gene. Therefore, an ultrasound gene transfer system, known as sonoporation, has attracted attention. This method allows less invasive and location-specific gene transfection, and it is known that micro-bubbles improve gene transfection rates. Genes are thought to be inducted into cells by the collapse of cavitation bubbles or micro-bubbles [4]. However, the mechanism and optimal induction conditions have not yet been fully clarified. In this research, we examined the availability of forming DNA/Block copolymer micelle. By forming micelle, DNA is compacted and the stability of DNA is improved. Therefore, it is expected that DNA become able to pass through a hole on cells easily and the expression ability of genes is advanced.

II. Materials and Methods

A. Experimental System

Fig.1 shows the experimental apparatus. Mouse fibroblast cell line (NIH3T3) is cultured on the bottom of 24-well plate. We add plasmid DNA and Micro-bubble to culture solution (D-MEM; FBS: 10%; PS: 1%) and then irradiate ultrasonic plane wave from above the cells. We use GFP plasmid as reporter gene, and Sonazoid® as micro-bubble.

Ultrasonic plane wave is emitted from the piezoceramic transducer (PZT) by impressing the amplified sinusoidal signal from the function generator (NF, WF1944A). We use E&I, 2100L as an amplifier. This piezoceramic is flat disk shape and the diameter is 12mm. The direction between the surface of transducer and the bottom of 24-well plate is 3.0mm. The frequency of the signal is 2.0MHz, which is the resonant frequency of Sonazoid®. For limiting damage to cells, we irradiate burst wave ultrasound, whose Duty Cycle is 10% (40/360). Reflected wave is blocked by putting 24-well plate on the water bath and setting acoustic absorbent material under it.

C.T. Lim and J.C.H. Goh (Eds.): WCB 2010, IFMBE Proceedings 31, pp. 1117 1120, 2010.
www.springerlink.com

B. *Ultrasound Intensity*

For the sake of computing the intensity of ultrasound, measurement of sound pressure is done. The transducer is sunk in deggased water and we measure the sound pressure 3.0mm under the surface of piezoceramic with needle hydrophone (production of imotec Messtechnik co. Type 80-0.5-4.0). This measurement is one-dimensional, because the sound pressure distribution made by a flat disk piezoceramic can be thought concentric. Therefore, the axis of measurement is set to pass through the center of piezoceamic. The measurement range is 16mm, which is the diameter of the one well of 24-well plate. The intensity of ultrasound is calculated based on this sound pressure measurement.

C. *Polyplex Micelle*

Micelle is formed by combining DNA and block copolymer (Fig.2). Block copolymer is composed of polyethyleneglycol-group and poly-lysine. In solution, lysine is positive charge, and plasmid DNA is negative charge. Therefore, poly-lysine and DNA interact with each other electrically, and block copolymer and DNA form polymer micelle (Fig.3) [5]. By forming polymer micelle, DNA is compacted [6] and the stability of DNA is improved [7].

Figuration of polymer micelle is controlled by N/P ratio, which is the ratio of amount of positive charge to amount of negative charge. When N/P ratio is high, polymer micelle is small and stability is high, but gene expression is low [8]. In this study, we adopt troid-shaped polymer micelle, which means N/P ratio is 1.5. The size of this polymer micelle is about 300nm.

D. *Confirming the Stability of DNA by Electrocataphoresis*

Naked DNA is attacked by nucleolytic enzyme in serum-containing medium [7] and loses ability of expressing, but this attack can be blocked by forming polymer micelle. Here, we confirm this stability improvement by gel electrocataphoresis.

Plasmid DNA in solution has supercoil (SC) structure. However, if DNA is attacked by nucleolytic enzyme and suffers a loss in at least one of bases, this structure collapses and plasmid DNA has an open circular (OC) structure. These two types of DNA, supercoil and open circular, can be separated by electrophoresis. Each naked DNA and polymer micelle is added to culture medium solution we use in ultrasound exposure experiment. After 15, 30, 60 minutes DNA is cataphoresed. Fig.4 shows the result. SC is the set of plasmids which have supercoil structure. These plasmids are not attacked by enzyme. OC is the one of plasmids which have open circular structure. These are attacked in at least one of bases. Fig.4 shows that most of Naked DNA is attacked by enzyme in 15 minutes. On the other hand, some polymer micelle DNA is immune to this attack for 60 minutes. This means improvement of stability of DNA is realized by forming polymer micelle.

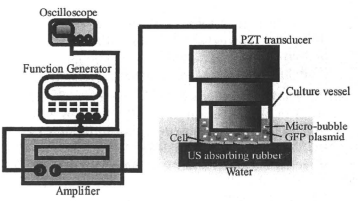

Fig. 1 Experimental apparatus

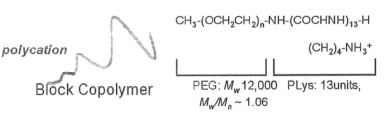

Fig. 2 Block copolymer and its structural fomula [5]

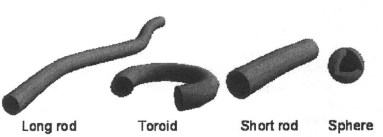

Fig. 3 Polymer micelle [5]

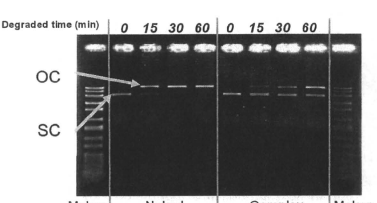

Fig. 4 Electrophoresis

III. Results and discussions

Each naked DNA and polymer micelle is added to culture medium with micro-bubble, and then we irradiate ultrasound. Experimental conditions are set as follows: plasmid density is 15μg/ml, number density of micro-bubble is 1.7×10^5 count/mm^3, ultrasound intensity is 5.08 W/cm^2, ultrasound exposure time is 60 seconds, and sample number is 12. Gene induction ratio is measured with flow cytometry in 48 hours after ultrasound exposure, since GFP plasmid expression achieves a peak in 48 hours after plasmids induction. Result (Fig.5) shows that gene induction ratio is doubled by forming polymer micelle. Therefore, the availability of forming polymer micelle is confirmed.

This result shows that gene induction ratio is doubled by forming polymer micelle. Forming polymer micelle has two availabilities. First, the size of DNA can be compacted. Normally, plasmid DNA in solution has supercoil structure or open circular structure in solution. Plasmid DNA we use in experiment is composed of about 6000 base pairs (that means the circle of this plasmid is about 2μm), so the size of plasmid DNA is up to 1μm if DNA is expandes absolutely. On the other hand, polymer micelle DNA is, in our study, about 300nm. Therefore, it can be considered that polymer micelle DNA can pass through the hole on cells more easily than naked DNA.

Second, the stability of DNA is improved. Naked DNA is attacked by nucleolytic enzyme in serum-containing medium. In our experimental system we use serum-containing medium when ultrasound is emitted to cells. Therefore, by forming polyplex micelle, the attack by enzyme can be blocked, and the amount of DNA which has the ability of expressing is advanced. We confirm this effect, that is, the blocking of enzyme attack enhanced gene induction ratio, by gene induction experiment without serum.

Naked DNA is added to culture medium with micro-bubble, and then exposure ultrasound. Medium of one sample contains 10% of FBS and 1% of penicillin, while that of the other does not contains FBS and penicillin. After ultrasound exposure, these medium is eliminated and culture medium which contains FBS (10%) and penicillin (1%) is added. This is because cells cannot live for 48 hours without FBS and penicillin. Experimental conditions are set as follows: plasmid density is 15μg/ml, number density of micro-bubble is 1.7×10^5 count/mm^3, ultrasound intensity is 5.08 W/cm^2, ultrasound exposure time is 60 seconds, and sample number is 12. Gene induction ratio is measured 48 hours after ultrasound exposure.

Fig.6 shows the result. It is clear that under serum free condition gene induction ratio is higher than that of with serum medium. Therefore, it can be said that the attack of nucleolytic enzyme diminishes gene induction efficiency and blocking this attack by forming polymer micelle is effective.

The one availability of polymer micelle, that is, the stability enhancement, is demonstrated to be effective to sonoporation. The other availability, compacting the size of DNA, must be demonstrated to be effective by some experiment. However, such kind of experiment has yet to be done.

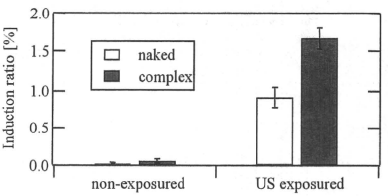

Fig. 5 Gene induction ratio by Naked DNA and polymer micelle

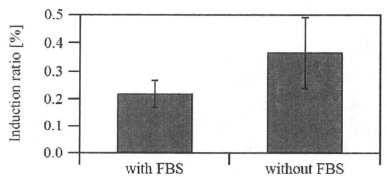

Fig. 6 Gene induction ratio with and without FBS

IV. Conclusion

By forming polymer micelle, stability of DNA in culture medium is improved. This was confirmed by electrocataphoresis. Then we proved that gene induction ratio is doubled by forming polymer micelle. This shows that polymer micelle is available.

Acknowledgment

This work was partially supported by a grant for the Center for NanoBio Integration (CNBI) and Translational Systems Biology and Medicine Initiative (TSBMI), from the Ministry of Education, Culture, Sports, Science and Technology of Japan.

REFERENCES

1. Alexander P, Inder M. V et al. (2001) GENE THERAPY: Promises and Prob-lems. Annu. Rev. Genomics Hum. Genet 2:177-211
2. Weaver J. C, Chizmadzhev, Y. A(1996) Theory of electroporation: A review. Bioelectrochemistry and Bioenergetics 41:135-160
3. Audouy S, Hoekstra D (2001) Cationic lipid-mediated transfection in vitro and in vivo. Molecular Membrane Biology 18:129-143
4. Okada K et al. (2005) A basic study on sonoporation with microbubbles exposed to pulsed ultrasound. J. Med Ultrasonics 32:3-11
5. Itaka K et al.(2009) Recent development of nonviral gene delivery systems with virus-like structures and mechanisms. European Journal of Pharmaceutics and Biopharmaceutics 71:475-483
6. Katayose S, Kataoka K (1997) Water-Soluble polyion complex associates of DNA and poly(ethylene glycol)-poly(L-lysine) block copolymer. Bioconjugate Chem 8:702-707
7. Katayose S, Kataoka K (1998) Remarkable increase in nuclease resistance of plasmid DNA through supermolecular Assembly with poly(ethylene glycol)-poly(L-lysine) block copolymer. Journal of Phamaceutical Science 87-2:160-163
8. M Harada-Shiba et al. (2002) Polyion complex micelles as vectors in gene therapy-pharmacokinetics and in vivo gene transfer. Gene Ther 6:407-414

Author: Akio Okamoto
Institute: The University of Tokyo
Street: 7-3-1, Hongo, Bunkyo ward
City: Tokyo
Country: Japan
Email: a-okamoto@fel.t.u-tokyo.ac.jp

キャビテーションに関するシンポジウム(第 15 回)
2010.11.22-23・堺市

マイクロバブルを援用した超音波遺伝子導入法の高効率化

Efficiency Improvement of Microbubble-Enhanced Sonoporation

○岡本 旭生(東大院)　橘 理恵(東大院)　葭仲 潔(東大工)　長田 健介(東大工)　高木 周(東大工)
片岡 一則(東大工)　鄭 雄一(東大工)　松本 洋一郎(東大工)

AkioOkamoto, Department of Mechanical Engineering, The University of Tokyo, 7-3-1, Hongo, Bunkyo ward, Tokyo, Japan
Rie Tachibana, Department of Mechanical Engineering, The University of Tokyo, 7-3-1, Hongo, Bunkyo ward, Tokyo, Japan
Kiyoshi Yoshinaka, Department of Bioengineering, The University of Tokyo, 7-3-1, Hongo, Bunkyo ward, Tokyo, Japan
Kensuke Osada, Department of Materials Engineering, The University of Tokyo, 7-3-1, Hongo, Bunkyo ward, Tokyo, Japan
Shu Takagi, Department of Mechanical Engineering, The University of Tokyo, 7-3-1, Hongo, Bunkyo ward, Tokyo, Japan
Kazunori Kataoka, Department of Bioengineering, The University of Tokyo, 7-3-1, Hongo, Bunkyo ward, Tokyo, Japan
Chung Ung-il, Department of Bioengineering, The University of Tokyo, 7-3-1, Hongo, Bunkyo ward, Tokyo, Japan
Yoichiro Matsumoto, Department of Mechanical Engineering, The University of Tokyo, 7-3-1, Hongo, Bunkyo ward, Tokyo, Japan

Sonoporation is a recently developed system for gene induction that uses ultrasound. Micro-bubbles are known to aid gene transfection through the introduction of genes into cells by the collapse of cavitation-bubbles (or micro-bubbles). However, the underlying mechanism and optimal introduction conditions have not been clarified in detail. In this research, we improved the gene introduction rate by optimizing burst waveshape of ultrasound and forming DNA/Block copolymer micelles. Micelle formation compacts the DNA and enhances its stability, thereby facilitating the passage of greater amounts of DNA through holes in the cell surface and improving gene expression. Our results show that gene induction ratio is enhanced as the exposed time per pulse and non-exposed time per pulse increase. The gene induction ratio is doubled by the formation of polymer micelles (from ~1% to ~2%), thereby confirming that the system is capable of generating polymer micelles for introducing DNA into cells.

Key Words:　Cavitation, Gene therapy, Cellular membrane, Bubble, Polymer micelle

1. はじめに

遺伝子治療とは，異常遺伝子を持つ細胞に対して新たに遺伝子を導入し，細胞の機能を正常化することで病気を治療する方法である．現在までに確立されている遺伝子導入法は侵襲性，副作用の危険性といった問題点を抱えており，低侵襲かつ副作用のない超音波遺伝子導入法が着目されている．超音波遺伝子導入法は超音波照射により細胞膜に一時的な小孔を物理的に生じさせることで遺伝子導入を実現する手法であり，マイクロバブルの援用により導入の効率が向上するという知見がある[1]．マイクロバブル援用超音波遺伝子導入法では超音波照射により生じるマイクロバブルの振動，崩壊といった現象を用いて細胞膜に小孔を一時的に生じさせ，遺伝子導入を実現していると考えられているが，[2]詳細な機序は不明である．また，遺伝子導入効率が他手法に比べ低いという問題がある．

超音波遺伝子導入法における細胞への小孔形成を評価した先行研究より，全細胞の 60%程度に小孔が形成される条件においても遺伝子導入率は 0.1%程度であることが示されている[3]．本研究は小孔形成細胞に対し効率的に遺伝子を導入する手法の開発を目的とし，超音波照射条件を最適化し，マイクロバブルの細胞に対する寄与を増大させる．また，遺伝子の高分子ミセル化によりサイズを縮小し安定性を向上させた上で超音波照射実験を行う．

2. 遺伝子導入実験システム

2-1 実験装置　超音波遺伝子導入実験装置の概略図を Fig.1 に示す．マウス性繊維芽細胞系 NIH3T3 を細胞培養容器に培養する．細胞培養液として D-MEM (Dulbecco's Modified Eagle Medium) に，血清である FBS を 10%，抗生物質である PS (penicillin-streptomycin) を 1%加えたものを用いる．ウェル内の細胞培養液に導入遺伝子とマイクロバブルを混和し，平面超音波を上方より照射する．導入遺伝子は緑色蛍光蛋白質(GFP)プラスミドを，マイクロバブルは Sonazoid[R]を用いる．平面超音波は直径 12 mm の円盤状のピエゾトランスデューサにファンクションジェネレータで発生させた信号をアンプで増幅し入力することで照射する．超音波の周波数は Sonazoid[R]の共振周波数である 2.0 MHz とし，細胞培養容器より 3 mm 上方より照射する．細胞へのダメージを抑制するため照射超音波の波形をバースト波形とする．水槽内にて細胞培養容器を吸音材の上に設置することで超音波の反射を防ぐ．遺伝子濃度を 15 μg/ml，マイクロバブル数密度を 1.7×10^5 /mm^3，サンプル数を 12 とする．

2-2 遺伝子導入率測定　GFP プラスミドが導入された細胞は細胞内で緑色蛍光タンパク質(GFP)を生成するため，遺伝子が導入された細胞が判別可能となる(Fig.2)．細胞内における GFP の生成量は遺伝子導入後 48 時間後にピークに達する為，超音波照射から 48 時間後にフローサイトメトリにより遺伝子導入率を測定する．フローサイトメータの細い流路に細胞を一個ずつ流し，レーザー光をあて，その散乱光により流路を流れた全

細胞数，および遺伝子導入細胞数を測定する．全細胞に対する遺伝子導入細胞の割合を遺伝子導入率と定義する．

2-3 細胞生存率測定法 本手法の細胞への毒性を評価するため，細胞の生存率を細胞毒性試験試薬 Cell Counting Kit 8 (以下 CCK8)を用いて測定する．CCK8 は生細胞の代謝により還元され，橙色の formazan が生成される．formazan 生成量は生細胞数に比例し，溶液中の formazan 量と溶液の吸光度も比例する．したがって，CCK8 を加えた細胞培養液の吸光度からサンプルの生存率を求めることができる．超音波照射を行わない細胞の培養液に formazan を加えたものをコントロールとし，コントロールの吸光度とサンプル培養溶液の 450 nm の吸光度を比較することで生存率を求める．遺伝子導入率と同じく超音波照射から 48 時間後に細胞培養液に CCK8 を加え，3 時間程度呈色反応させた後，吸光度を測定する．

3. バースト波形をパラメータとした遺伝子導入実験

3-1 バースト波形依存性測定実験 超音波の波形をバーストとすることで，Fig.3 のように一定の照射時間に対し照射休み時間を設けることになり，連続波に比べ細胞へのダメージが抑制されるという知見が得られている[4]．本研究ではこのバースト波形に着目し，遺伝子導入率のバースト波形に対する依存性を調査する．1 パルスにおける照射時間，照射休み時間，および単位時間におけるパルス数である PRF をバースト波形のパラメータとし，それぞれに対する遺伝子導入率の依存性を 2 章に記した方法で測定する．ただし，1 パルス当たりの照射時間，照射休み時間の単位を cycle とする．本研究では 2.0 MHz の超音波を用いるため，1cycle は 0.5 μs に相当する．

まず 1 パルスにおける照射時間に対する依存性を調べるため，照射休み時間を 100 cycle と固定し，照射時間を 10, 100, 1000 cycle と変化させたときの遺伝子導入率を測定する．照射時間に応じて全照射時間を変化させ，全照射時間における投入エネルギー量を固定する．照射時間 10 cycle のサンプルに対し全照射時間を 110 s, 100 cycle のものに対し 20 s, 1000 cycle としたものに対し 11 s とする．照射休み時間に対する依存性についても同様に，照射時間を 100 cycle と固定し，照射休み時間を 10, 100, 1000 cycle と変化させる．全照射時間は，照射休み時間 10 cycle のサンプルに対し 11 s, 100 cycle のものに対し 20 s, 1000 cycle のものに対し 110 s とする．また，照射時間と照射休み時間の比である Duty 比を 10%と固定したときの，PRF に対する依存性を測定する．PRF を 50, 500, 5000, 50000 Hz と変化させ，全照射時間を 60 s とする．以上の実験において超音波強度を 5.0 W/cm^2 とする．

3-2 結果と考察 Fig.4 (a),(b)は照射時間をパラメータとした実験の結果である．これより，照射時間が長いほど，遺伝子導入率が向上し，生存率は低下していることが判る．これは，照射時間の増大に伴い 1 パルス間に生じる細胞膜表面の小孔のサイズが大きくなることに起因すると考察される．

Fig.5 (a),(b)は照射休み時間をパラメータとした実験の結果を示している．照射休み時間の増加に伴い，遺伝子導入率，細胞生存率ともに向上していることがわかる．これは，十分な照射休み時間を設けることで細胞へのダメージが抑制されたため，小孔が生じ遺伝子が導入された細胞が生存できるようになったことに起因すると考察される．

Fig.6 (a),(b)はPRFをパラメータとした結果である．PRF が小さいほど遺伝子導入率が高いことがわかる．PRF が低いほど照射時間，照射休み時間ともに長くなるため，この結果は照射時間，および照射休み時間依存性と一致するといえる．また，PRF が小さいほど細胞生存率は低下していることがわかる．これは，低 PRF で照射時間が長くなり，細胞へのダメージが大きくなるためと予想される．

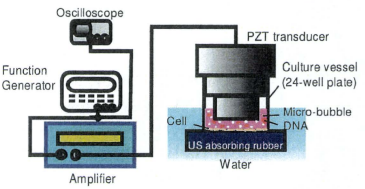

Fig.1 Experimental apparatus

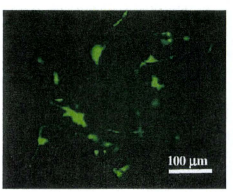

Fig.2 Fluorescent observation of GFP

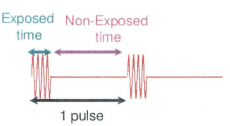

Fig.3 Burst waveshape

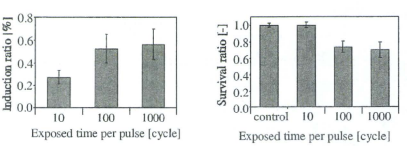

Fig.4 Dependency on exposed time per pulse

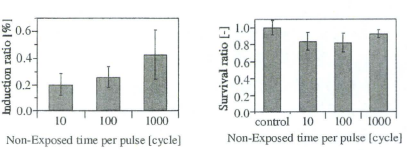

Fig.5 Dependency on Non-Exposed time per pulse

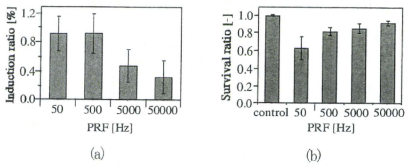

Fig.6 Dependency on PRF

4. プラスミドの高分子ミセル化

4-1 高分子ミセル　遺伝子の高分子ミセル化にはブロック共重合体(Fig.7)を用いる. ブロック共重合体はポリエチレングリコール基の先端にリジンが13個結合したものである. プラスミドは溶液中で負に帯電しているのに対し, リジンは正に帯電している. そのため, プラスミドはブロック共重合体中のリジンと電気的に相互作用し, 溶液中で高分子ミセル(Fig.8)を形成する[5].

細胞培養液中の核酸分解酵素が機能するとプラスミドの塩基配列が損なわれる. タンパク質発現に必要となる塩基が損なわれるとプラスミドは発現性を失う. 高分子ミセル化されたプラスミドは核酸分解酵素の影響を受けにくくなるため, 培養液中での安定性が向上する[6]. また, 高分子ミセル化によりプラスミドのサイズが縮小される[6]. そのため, 超音波照射により生じた細胞表面の小孔を通過しやすくなることが期待される.

高分子ミセルの形状, 性質を制御するパラメータとしてN/P比を用いる. N/P 比は, プラスミドの持つ負電荷の総量に対する, ブロック共重合体の持つ正電荷の総量の比と定義される. N/P 比が大きいほど高分子ミセルは小さくなり, 同時に安定性も向上するが, 発現性は低下する[7]. 本研究では N/P 比を 1.5 とする. N/P 比が 1.5 の状態では高分子ミセルはドーナツ型となり, このときのサイズは 300nm 程度である. 本研究で用いるプラスミドはおよそ 6000 の塩基対より構成され, 最大で 1 μm 程度の広がりを持つため, 高分子ミセル化によりサイズ縮小が実現されているといえる.

4-2 電気泳動による遺伝子の安定性の確認　前述した高分子ミセル化によるプラスミドの安定性向上の効果をゲル電気泳動により評価する. プラスミドは溶液中でスーパーコイルと呼ばれる高次構造をとるが, 核酸分解酵素の機能で塩基が損なわれることによりオープンサーキュラーやリニアへと高次構造が変化する[8]. 異なる高次構造のプラスミドは電気泳動で分離できるため, 高次構造の時間変化を可視化することで核酸分解酵素存在下でのプラスミドの安定性を評価することができる.

通常のプラスミドまたは高分子ミセル化プラスミドを細胞培養溶液に加え, 一定時間反応させた後, EDTA,DDTA を溶液に加えミセルを解離させ, 電気泳動を行う. 反応時間は 0, 15, 30, 60 分とし, プラスミド濃度は遺伝子導入実験と等しく 15 μg/ml とする. 電気泳動の結果を Fig.9 に示す. 図中の SC はスーパーコイル, OC はオープンサーキュラーの高次構造をとるプラスミドである. 通常のプラスミドは 15 分以内にほぼすべてがオープンサーキュラーに変化しているのに対し, 高分子ミセル化したものはこの変化が抑制されていることが分かる. これはプラスミドの高分子ミセル化により細胞培養液中での安定性が向上していることを示している.

4-3 高分子ミセル化プラスミド導入実験　通常のプラスミド, または高分子ミセル化したプラスミドを細胞に導入する実験を行う. 実験は 2 章に記した方法で行い, 超音波強度を 5.1 W/cm^2 とする. 結果を Fig.10 に示す. 遺伝子の高分子ミセル化により, 遺伝子導入率が向上していることがわかる. これはプラスミドの高分子ミセル化により超音波遺伝子導入法の高効率化が可能であることを示している.

4-4 血清のない状態での遺伝子導入実験　前述したとおり, DNA の高分子ミセル化により, DNA は細胞培養液中に存在する核酸分解酵素の影響を受けにくくなり, 安定化する. 本実験系における核酸分解酵素の影響を, 血清のない状態で Naked の遺伝子を導入する実験を行うことで評価する.

24 ウェルプレートに細胞を培養し, 培養液を吸引除去し, FBS を 10%, PS を 1%含む D-MEM を加えたもの, 及び両者を含まない D-MEM を加えたものを用意する. これらのサンプルに対し 2 章に記した方法で Naked の DNA を導入する実験を行う. 超音波強度を 5.1 W/cm^2 とする. 実験結果 (Fig.11) より, 血清を含む培養液を用いると遺伝子導入率が低下していることがわかる. これは, 核酸分解酵素の機能により遺伝子導入が妨げられていることを示している. DNA を高分子ミセル化することで核酸分解酵素の機能を制限することが, 遺伝子導入率の向上に寄与したと考えられる.

高分子ミセル化によるメリットの 1 つである遺伝子の安定化が遺伝子導入率向上に寄与していることを本実験で検証した. しかし, もう1つのメリットであるサイズ縮小が遺伝子導入率向上に寄与していることは検証されていないため, 粒子導入実験などにより検証する必要がある.

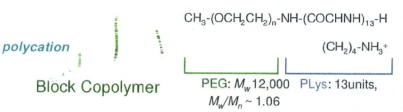

Fig.7 Block copolymer and its structural fomula [5]

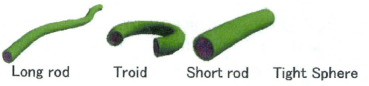

Fig.8 Polyplex micelle [5]

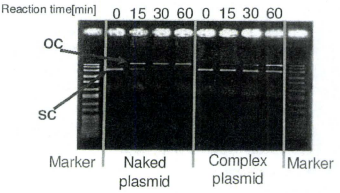

Fig.9 Electrophoresis

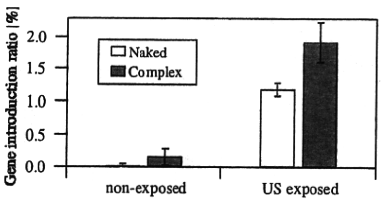

Fig.10 Gene introduction ratio by Naked DNA and micelle

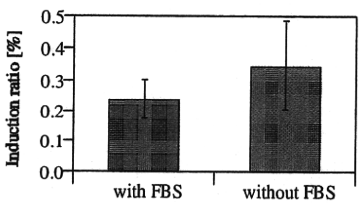

Fig.11 Gene induction ratio with and without FBS

5. 結論

本研究ではマイクロバブルを援用した超音波遺伝子導入法の高効率化を目指し，以下の知見を得た．

超音波のバースト波形をパラメータとした遺伝子導入実験より，1 パルスにおける照射時間が長いほど，照射休み時間が長いほど遺伝子導入効率が向上することを示した．PRF をパラメータとした実験では低 PRF で遺伝子導入率が高くなることが示され，照射時間，照射休み時間依存性と一致した．

DNA のサイズ縮小，および安定化により遺伝子導入効率が向上することを，高分子ミセル化 DNA 導入実験により示した．

謝辞

本研究の一部は、ナノバイオ・インテグレーション研究拠点(CNBI)，システム疾患生命科学による先端医療技術開発拠点 (TSBMI)の支援を受けて実施したものである．ここに記して謝意を表する．

参考文献

[1] Hirayama K et al., Proc. of 6th ISTU, 2006
[2] Okada K et al., "A Basic Study on Sonoporation with Microbubbles Exposed to Pulsed Ultrasound," J. Med Ultrasonis, Vol. 32, pp. 3-11, 2005.
[3] Tachibana R et al., Proc of 9th ISTU, 2009
[4] Hun P et al, Study of Sonoporation Dynamics Affected by Ultrasound Duty Cycle", Ultrasound Med Bio, Vol. 31, pp. 849-856
[5] Itaka K et al., "Recent Development of Nonviral Gene Delivery Systems with Virus-like Structures and Mechanisms," European Journal of Pharmaceutics and Biopharmaceutics, Vol. 71, pp. 475-483, 2009.
[6] Katayose S et al., "Remarkable Increase in Nuclease Resistance of Plasmid DNA through Supermolecular Assembly with Poly(ethylene glycol)-poly(L-lysine) Block Copolymer," Journal of Phamaceutical Science, Vol.87-2, pp. 160-163, 1998.
[7] M Harada-Shiba et al., "Polyion Complex Micelles as Vectors in Gene Therapy-pharmacokinetics and in vivo Gene Transfer," Gene Ther. Vol.6, pp. 407-414, 2002.
[8] Benjamin Lewin, "遺伝子(上)," 東京化学同人

Reprinted from

JAPANESE JOURNAL OF
APPLIED
PHYSICS

REGULAR PAPER

Production of Local Acoustic Radiation Force to Constrain Direction of Microcapsules in Flow

Kohji Masuda, Nobuyuki Watarai, Ryusuke Nakamoto, and Yusuke Muramatsu

Jpn. J. Appl. Phys. **49** (2010) 07HF11

Japanese Journal of Applied Physics 49 (2010) 07HF11 **REGULAR PAPER**

Production of Local Acoustic Radiation Force to Constrain Direction of Microcapsules in Flow

Kohji Masuda*, Nobuyuki Watarai, Ryusuke Nakamoto, and Yusuke Muramatsu

Graduate School of Bio-Applications and Systems Engineering, Tokyo University of Agriculture and Technology, 2-24 Nakacho, Koganei, Tokyo 184-8588, Japan

Received November 25, 2009; revised March 31, 2010; accepted April 8, 2010; published online July 20, 2010

We have ever reported our attempt to control the direction of microcapsules in flow by acoustic radiation force. However, the diameter of capsules was too large to be applied *in vivo*. Furthermore, the acoustic radiation force affected only the focal area because focused ultrasound was used. Thus, we have improved our experiment by using microcapsules as small as blood cells and introducing a plane wave of ultrasound. We prepared an artificial blood vessel including a Y-form bifurcation established in two observation areas. Then, we newly defined the induction index to evaluate the difference in capsule density in two downstream paths. As a result, the optimum angle of ultrasound emission to induct to the desired path was derived. The induction index increased in proportion to the central frequency of ultrasound, which is affected by the aggregation of capsules to receive more acoustic radiation force.

DOI: 10.1143/JJAP.49.07HF11

1. Introduction

Many researches of drug delivery system have been proposed by applying microcapsules or microbubbles as a drug carrier in the human body.[1–4] The existence of capsules (or bubbles) improves the introduction efficiency to the target area by making use of sonoporation.[5] While the lifetime of the microbubbles is several minutes, we consider that the microcapsules are more suitable for use with various types of delivery. However, because of the diffusion of capsules after injection, it is difficult to deliver capsules from the point of injection to desired target area through bifurcations of blood vessel. If the behavior of capsules could be controlled and constrained in terms of direction, the introduction efficiency would be enhanced. Owing to acoustic radiation force,[6–9] which is a physical phenomenon where an acoustic wave pushes an obstacle along its direction of propagation, we have previously reported our attempt to propel microcapsules in water.[10] We have elucidated the conditions of sound pressure, flow velocity, and diameter of capsules for the active path selection of capsules in an artificial blood vessel. However, because we used capsules with diameters of more than 60 μm, they were too large to be applied *in vivo*. Furthermore, we also used focused ultrasound to concentrate the acoustic radiation force, which affected only the focal area. Because the acoustic radiation force is proportional to the square of the size of a capsule, a larger acoustic field can produce more radiation force to propel a capsule in flow. Thus, we have improved our experiment to adopt capsules as small as blood cells with a plane wave of ultrasound.

Considering micrometer-sized microcapsules, upon ultrasound exposure, they are oscillated to produce Bjerknes force and aggregate with each other[11,12] if the frequency of ultrasound is near their resonance frequency. We already confirmed the aggregation of capsules in a straight flow when acoustic radiation force was produced in the oncoming direction with MHz-order frequencies.[13] However, frequency dependence was not elucidated when capsules were propelled in flow by the radiation force.[14,15] In this study, we investigated the optimal conditions to propel microcapsules in flow using a plane wave of ultrasound with various frequencies.

*E-mail address: masuda_k@cc.tuat.ac.jp

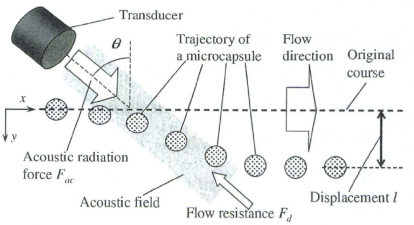

Fig. 1. Trajectory of microcapsule in flow under ultrasound emission.

2. Principle

Assuming that the shape of capsules is spherical and they are located in a uniform acoustic field, an acoustic radiation force acts to propel a capsule in the direction of acoustic propagation as per the following equation:[15,16]

$$F_{ac} = \pi r^2 Y_p P, \tag{1}$$

where P is the mean energy density of the incident wave, Y_p is a dimensionless factor called the radiation force function that depends on the scattering and absorption properties of the capsule, and r is the radius of the capsule. Here, the effect of ultrasound frequency in F_{ac} is not clear because Y_p does not include an item of frequency.[17]

When the microcapsules are placed in flow, a capsule should receive flow resistance. If the acoustic radiation force is greater than the flow resistance, the trajectory of the capsule is curved, as shown in Fig. 1. At a positive value of angle θ in Fig. 1, a capsule is propelled in the y-direction with lower flow resistance than at a negative value of angle θ. At a larger value of angle θ, although a capsule passes through the acoustic field for a longer period, the radiation force propels the capsule in the x-direction more than in the y-direction. In Fig. 1, although the shape of the acoustic field is expressed as a square, it is measured before the experiment.

3. Experimental Methods

3.1 Diameter distribution of microcapsules

We used F-04E microcapsules (Matsumoto Oil), which have

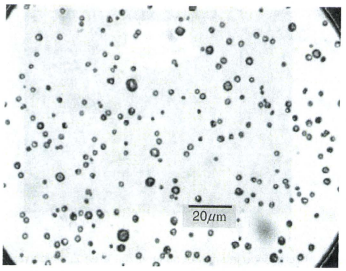

Fig. 2. Microscope image of selected F-04E microcapsules with a diameter of less than 5 μm.

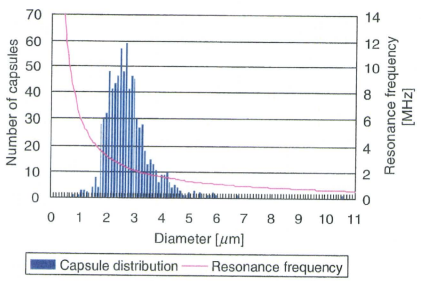

Fig. 3. (Color online) Diameter distribution of F-04E microcapsules plotted with the resonance frequency of eq. (2) according to the diameter.

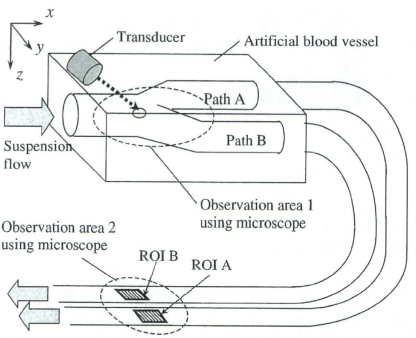

Fig. 4. Schematic view of artificial blood vessel with the locations of the two observation areas.

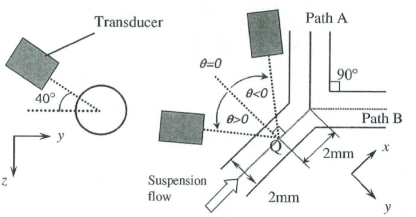

Fig. 5. Position configuration between a transducer and the artificial blood vessel near the bifurcation.

a shell made of poly(vinyl chloride) (PVC), a specific gravity of 0.0225, and an average diameter of 4 μm. They contain isobutene inside and are stable at room temperature. We selected only those microcapsules with a diameter of less than 5 μm by using microsieves. Figure 2 shows a microscope image of the selected microcapsules. We measured the diameter of more than 800 capsules through five microscope images to elucidate the diameter distribution of the capsules. Figure 3 shows the diameter distribution of the capsules as bars, where most of the diameters of capsules are between 2 and 3.5 μm. Since the solid line in Fig. 3 indicates the resonance frequency f of the microbubble, which is calculated as per eq. (2),[7,18] the resonance frequency ranges between 2 and 4 MHz according to the diameter.

$$f = \frac{1}{2\pi r}\sqrt{\frac{3kP}{\rho}}, \tag{2}$$

where k is the ratio of specific heats. However, because of the shell, the resonance frequency of microcapsules should be higher than that of microbubbles. According to a mathematical simulation,[19] the theoretical resonance frequency of microcapsules is estimated to be between 5 and 7 MHz with a diameter of 4 μm. Thus, the behavior of capsules is considered to be mostly affected by MHz-order frequencies.

3.2 Observation of capsule behavior

We have also prepared an artificial blood vessel made of poly(ethylene glycol) (PEG), including a Y-form bifurcation, as shown in the schematic view of Fig. 4. The external size was $85 \times 55 \times 10\,\text{mm}^3$ and the inner diameter of the paths was 2 mm. The blood vessel was placed in the bottom of a water tank, which was filled with water. Because the acoustic impedance of PEG (sound velocity: 1540–1560 m/s, density: 1.27 g/mL) is similar to that of water, the energy of ultrasound in water reaches the path with high efficiency. As shown in Fig. 4, optical images of observation areas 1 and 2 were recorded independently using a microscope (Omron KH-7700) and an inverted microscope (Leica DMRIB), respectively.

Figure 5 shows the position configuration between a transducer and the artificial blood vessel near the bifurcation in observation area 1. The axis of the transducer was set at 40° from the $-y$ direction around the x-axis to prevent physical interference between the transducer and the edge of the water tank. The transducer included a flat ceramic disc with a diameter of 20 mm to emit a plane wave of ultrasound. We have prepared five transducers, which have their central frequencies at 0.5, 1, 2, 3, and 5 MHz, to compare the effect of resonance frequency. Figure 6 shows the two-dimensional distribution of sound pressure of the 3 MHz transducer, where the x-axis indicates the direction of

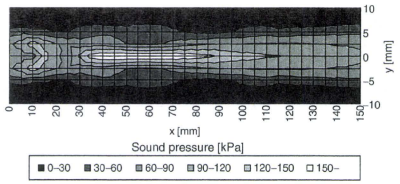

Fig. 6. Two-dimensional distribution of sound pressure of the 3 MHz transducer. (*x*-axis indicates the direction of ultrasound propagation, and the line of $x = 0$ corresponds to surface of the transducer).

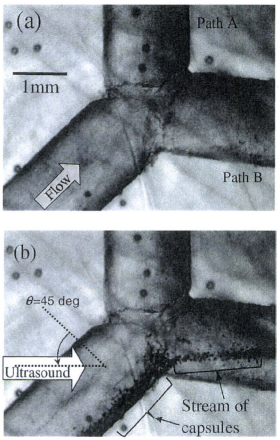

Fig. 7. Comparison of microscope images of observation area 1 (a) before and (b) after injection of capsule suspension (flow velocity: 20 mm/s, central frequency of ultrasound: 2 MHz, and maximum sound pressure: 400 kPa).

ultrasound propagation, and the line of $x = 0$ corresponds to the surface of the transducer. The shape of the highest sound pressure is wider than that of focused ultrasound.[10] Because the half width of the ultrasound beam ranges between 4 and 5 mm in above five transducers, the axis of the transducer was directed to point Q, as shown in Fig. 5, which was set to be 2 mm from the bifurcation point to the upstream course. The distance from the surface of a transducer to point Q was set to between 50 and 60 mm, so that point Q is included in the area of the highest sound pressure.

3.3 Evaluation of induction of capsules to the desired path

As shown in Fig. 7, when ultrasound was emitted, aggregations of capsules were clearly observed to enter path B rather than path A in observation area 1, whereas neither aggregations of capsules nor a significant difference between paths were observed without ultrasound. To evaluate the number of capsules that passed through each path, we extended the two paths using semitransparent tubes and

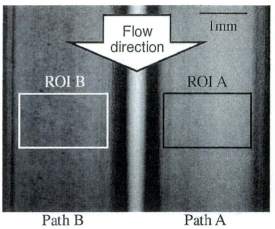

Fig. 8. Microscope images of observation area 2, which were taken at 300 fps after the injection of the capsule suspension in a flow velocity of 5 mm/s with an ultrasound emission of 2 MHz and a maximum sound pressure of 500 kPa.

established observation area 2, where both paths were observable in a single view. Figure 8 shows microscope images of observation area 2, which were captured using a high-speed camera (Casio EX-F1) attached to the microscope with an interval time of 3.3 ms (300 fps), when the capsule suspension was injected with a flow velocity of 5 mm/s with ultrasound emission of 2 MHz, and a maximum sound pressure of 500 kPa. Because of the limitation of optical magnification, although individual microcapsules cannot be distinguished, thicker suspension in path B was confirmed.

To measure the amount of microcapsules, we established two square regions of interest (ROI), the size of which is $1.8 \times 1.2\,\text{mm}^2$, in each path (ROIs A and B) and calculated the average brightness. In our previous paper[10] we evaluated the amount of capsules by defining the shadow index, which reflects the brightness change according to the existence of capsules in a ROI. However, the value of the shadow index cannot be compared between ROIs if there is an initial brightness difference between them. Thus, we newly defined the induction index by comparing two ROIs as follows.

Figure 9 shows the variations in brightness average in both ROIs upon injection of a capsule suspension with a flow velocity of 20 mm/s. Before the injection, the brightness was constant but there was a difference between the two ROIs. According to the appearance of capsules, after 7 s, the brightness of both ROIs decreased simultaneously. A significant different variation was confirmed upon ultrasound emission of 2 MHz and 500 kPa, which indicates that more capsules were inducted to ROI B after 28 s. According to disappearance of capsules, after 48 s, they returned to their initial brightness. Thus, calculating the subtraction of brightness with capsules from the initial brightness in each ROI, and comparing ROIs, we have defined the induction index ξ_B (%) of capsules to be inducted to path B rather than path A using the following equation:

$$\xi_B = \frac{(I_B - I_{B0}) - (I_A - I_{A0})}{(I_B - I_{B0}) + (I_A - I_{A0})} \times 100, \tag{3}$$

where I_{A0} and I_{B0} indicate the initial brightness average without capsules, and I_A and I_B indicate the brightness average with capsules, in ROI A and B, respectively. We confirmed that the induction index ξ_B reflects the relative ratio of capsules to pass through ROI B versus the total

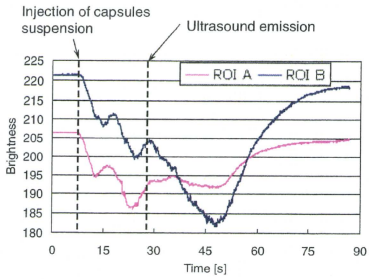

Fig. 9. (Color online) Variations in brightness average in ROIs A and B upon injection of a capsule suspension with a flow velocity of 20 mm/s, before and after ultrasound emission of a maximum sound pressure of 500 kPa and central frequency of 2 MHz.

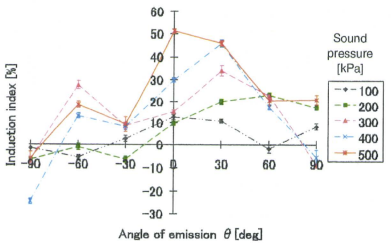

Fig. 10. (Color online) Induction index versus angle of emission with plane ultrasound of 3 MHz and flow velocity of 20 mm/s.

amount of capsules through our previous recordings movies,[10,13] in which we calculated the shadow index versus capsules density.

4. Results and Discussion

Figure 10 shows the induction index ξ_B versus the angle of ultrasound emission θ for five types of maximum sound pressure, a flow velocity of 20 mm/s, and a central frequency of 3 MHz. Here, the value of induction index was calculated from the sampled frames recorded with a high frame of 300 fps, while capsules appeared in the frame under ultrasound emission. The number of sampled frames was set to 300 frames, which depends on the duration of capsule appearance. When the sound pressure is less than 200 kPa, dominant induction to path B was observed in the positive angle of emission. When the sound pressure is more than 300 kPa, although capsule induction to path B was confirmed at an angle of emission of $-60°$, significant induction to path B was confirmed at an angle of emission of 30°. The optimum angle of ultrasound emission for induction to path B in the experiment was at an angle of 30°, which was used in the following experiment.

We measured the induction index upon emission of sinusoidal ultrasound with frequencies of 0.5, 1, 2, 3, and 5 MHz. Figures 11(a)–11(c) show the values of the induction

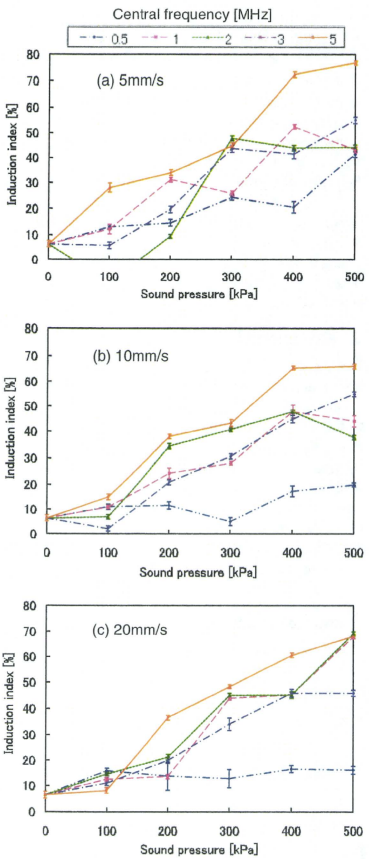

Fig. 11. (Color online) Induction index versus maximum sound pressure of plane ultrasound by the angle of emission of 30° in flow velocities of (a) 5, (b) 10, and (c) 20 mm/s, respectively.

index versus the maximum sound pressure, when the flow velocity was 5, 10, and 20 mm/s, respectively, where θ was fixed at 30°. Under every condition of flow velocity, the induction index increased in proportion not only to the sound pressure but also to the central frequency of the ultrasound. Regarding the central frequency, more capsules were inducted to the desired path when it was close to the resonance frequency, which is considered to be more than 5 MHz. We have considered that the result reflects the effect of aggregation of capsules.

Because capsules form aggregations under ultrasound emission, they should be equivalent to a larger volume than isolated capsules. When the frequency is near the resonance frequency, the capsules would be greatly oscillated to form

larger aggregations and to receive more acoustic radiation force in the direction of propagation. We have to investigate the behavior of capsules more precisely under various conditions of ultrasound.

From these results, using the higher pressure, higher frequency, and plane ultrasound, more capsules could be inducted to the desired path at the bifurcation of a blood vessel. In the next step, we are going to elucidate the behavior of capsules in flow theoretically before applying it to an *in vivo* experiment. The effect of acoustic streaming should be considered by using a higher frequency than 5 MHz. Meanwhile, we are going to develop a method to identify the precise location of bifurcations *in vivo* by detecting and constructing the three-dimensional shape of the blood vessel.

5. Conclusions

In this study, we realized active control of microcapsules with a diameter of less than 5 μm to constrain the direction in an artificial blood vessel. In a simple bifurcation, significant induction was confirmed when the angle of ultrasound emission was 30° from the rectangular of the flow to upstream. We confirmed that capsules were inducted into the desired path using the higher pressure, higher frequency, and plane ultrasound. For further analysis, the precise conditions necessary to realize active control of capsules in a complicated shape of blood vessel should be elucidated. Also, we are going to consider applications for future *in vivo* experiments.

Acknowledgment

This work was supported by Research and Development Committee Program of the Japan Society of Ultrasound in Medicine.

1) M. Watanabe, K. Chihara, K. Shirae, K. Ishihara, and A. Kitabatake: *Proc. 11th Symp. Ultrasonic Electronics, Kyoto, 1990*, Jpn. J. Appl. Phys. **30** (1991) Suppl. 30-1, p. 241.
2) N. de Jong, R. Cornet, and C. T. Lancée: Ultrasonics **32** (1994) 447.
3) K. Okada, N. Kudo, K. Niwa, and K. Yamamoto: J. Med. Ultrason. **32** (2005) 3.
4) H. Zheng, P. Dayton, C. Caskey, S. Zhao, S. Qin, and K. Ferrara: Ultrasound Med. Biol. **33** (2007) 1978.
5) Y. Yamakoshi, Y. Koitabashi, N. Nakajima, and T. Miwa: Jpn. J. Appl. Phys. **45** (2006) 4712.
6) Y. Yamakoshi: Jpn. J. Appl. Phys. **40** (2001) 1526.
7) H. Mitome: Jpn. J. Appl. Phys. **40** (2001) 3484.
8) T. Kozuka, K. Yasui, T. Tuziuti, A. Towata, and Y. Iida: Jpn. J. Appl. Phys. **47** (2008) 4336.
9) T. Kozuka, K. Yasui, T. Tuziuti, A. Towata, J. Lee, and Y. Iida: Jpn. J. Appl. Phys. **48** (2009) 07GM09.
10) K. Masuda, Y. Muramatsu, S. Ueda, R. Nakamoto, Y. Nakayashiki, and K. Ishihara: Jpn. J. Appl. Phys. **48** (2009) 07GK03.
11) Y. Yamakoshi and T. Miwa: Jpn. J. Appl. Phys. **47** (2008) 4127.
12) Y. Yamakoshi and T. Miwa: Jpn. J. Appl. Phys. **48** (2009) 07GK02.
13) K. Masuda, R. Nakamoto, Y. Muramatsu, Y. Miyamoto, K. Kim, and T. Chiba: Proc. 31st Annu. Int. Conf. IEEE Engineering in Medical and Biology Society, 2009, p. 295.
14) T. Lilliehorn, U. Simu, M. Nilsson, M. Almqvist, T. Stepinski, T. Laurell, J. Nilsson, and S. Johansson: Ultrasonics **43** (2005) 293.
15) T. Hasegawa, Y. Hino, A. Annou, H. Noda, and M. Kato: J. Acoust. Soc. Am. **93** (1993) 154.
16) F. G. Mitri: Wave Motion **43** (2005) 12.
17) T. Hasegawa, T. Kido, C. W. Min, T. Iizuka, and C. Matsuoka: Acoust. Sci. Technol. **22** (2001) 273.
18) M. Minnaert: Philos. Mag., Ser. 7 **16** (1933) 235.
19) K. Yasui, J. Lee, T. Tuziuti, A. Towata, T. Kozuka, and Y. Iida: J. Acoust. Soc. Am. **126** (2009) 973.

0916-2410/10/¥500/論文/JCLS
U0908-07

解　説　　医用超音波

模擬血管中を流れるマイクロカプセルに対する音響放射力とその影響

＝超音波による薬物伝送システム（DDS）のための基礎検討＝

東京農工大学　村松 悠佑・桝田 晃司

1．はじめに

現代の医療にとって投薬治療は必要不可欠な方法として用いられている反面、投薬効率や副作用など解決すべき問題も存在する。そのため、患部にのみ必要量の薬物を送る選択的薬物伝送システム（Drug Delivery System, DDS）の研究が注目されている。現在の主流は修飾基等による化学的DDSであるが、開発にかかる時間とコストが膨大で、しかも汎用性に乏しいという欠点がある[1]。それに対して中空マイクロカプセル中に薬物を含ませ、患部に届ける物理的DDSの研究も進められている[2]~[4]。

この方法は、薬物を含むマイクロカプセルを患部に届け、体外からの超音波照射によってカプセルを破壊することで目的部にのみに投薬を行う。カプセルに含まれる気体は血液中では優れた超音波感受性を持つため、体外からのモニタリングが容易であり、カプセルの検出と破壊を超音波のみによって行うことが出来る。またこの手法を化学的DDSと組み合わせることにより、カプセルに含ませる薬物を替えるだけで様々な投薬治療を低コストで行うことが出来るだけでなく、将来的には遺伝子導入[5]も可能になると考えられる。最近では、抹消血管さえも通過することが出来るマイクロカプセルが開発されている[6]ため、実現性は高いと考えられる。超音波とマイクロカプセルを用いたDDS実現のためには大きく分けて以下の４つの技術が必要になる。

① 多くのカプセルを目的部に誘導する技術
② 体内でカプセルを捕捉する技術
③ 捕捉されたカプセルを破壊する技術
④ 体内に注入されたカプセルのモニタリング技術

これまでの研究により、②では定在波を用いたマイクロカプセルの捕捉[7]~[9]、③では超音波の照射によるカプセルの崩壊[10]、さらには超音波音場内での気泡運動の観察や理論的考察[11]などが行われてきた。本研究室でも④の実現を目指し、超音波断層像の輝度情報からカプセル濃度を検出するシステムを開発[12]した。しかしながら、①に関しては体内に投与した後のカプセルは血流に任せるのみで、拡散によって目的部でのカプセル濃度は低くなるという問題が残っていた。

そこで我々は、分岐を有する模擬血管に超音波を照射することでカプセルに経路選択機能を付加できることを示し[13]、理論的検証を行った。本論文では超音波の音圧や、水流の流速などのパラメータ変化に伴うカプセル誘導の精度について光学的観測を行い、カプセルの誘導条件を算出した。

2．実験方法

2−1　マイクロカプセルとその懸濁液

本研究ではマイクロカプセルとして、松本油脂社製マイクロスフェアーF-80Eを用いた。このカプセルは熱可塑性高分子（AN系コポリマー）の殻を有し、炭化水素（イソブタン）を内包している。生分解性が無いため生体で使用することは出来ないが、本研究で用いる音圧及び流速の範囲で安定であるため採用した。またカプセルの直径は、通常のマイクロバブルよりも１桁大きい63~75 μmに統一した。本来であれば、赤血球（直径約8 μm）程度のサイ

※本記事は第29回超音波シンポジウムで発表された論文に基づいております。